Pergamon

Int. J. Solids Structures Vol. 32, No. 17/18, pp. 2627–2646, 1995

0020-7683/95 $9.50 + .00

0020-7683(94)00286-X

A MICROMECHANICAL MODEL FOR HIGH STRAIN RATE BEHAVIOR OF CERAMICS

G. RAVICHANDRAN and G. SUBHASH†
Graduate Aeronautical Laboratories, California Institute of Technology, Pasadena, CA 91125, U.S.A.

(*Received* 3 *February* 1994)

Abstract—A constitutive model applicable to brittle materials such as ceramics subjected to biaxial compressive loading is developed. The model is based on non-interacting sliding microcracks that are uniformly distributed in the material. Tension cracks nucleate and propagate from the tip of the sliding cracks in the direction of maximum applied compression when the stress-intensity factor reaches its critical value. For high strain rate deformation, the rate of crack growth is governed by a universal relation in dynamic fracture. The constitutive model provides strain components for plane deformation which consists of an elastic part and a part due to sliding and growth of the tension cracks. The failure of the material is linked to a critical density of damage and hence a critical length for the tension cracks. The constitutive model is used to study material behavior under uniaxial compressive constant strain rate loading. A critical strain rate beyond which the material would exhibit rate sensitivity is proposed. The model predicts the failure or peak strength to increase with increasing strain rate. For engineering ceramics, the rate sensitivity exponent is found to be a function of the relation between the rate of crack growth and the toughness of the material. The model predictions are compared with the rate-dependent behavior of a hot pressed aluminum nitride tested in uniaxial compression in the strain rate range of 5×10^{-6}–2×10^{3} s^{-1}.

1. INTRODUCTION

Brittle materials such as monolithic ceramics and ceramic composites are finding increasing applications and there is a need to design them for resistance to impact loading. An understanding of damage evolution under dynamic loading conditions is important in the analysis of structures made of brittle materials. In the absence of lateral confinement, failure of ceramics and ceramic composites under compression occurs at strains on the order of 1–2%. It has been observed that ultimate failure strength (impact or peak strength) of ceramics is rate sensitive in uniaxial compression; see for example, Lankford (1981) and Subhash and Ravichandran (1993). Past investigations have shown that damage in the form of microcracking and/or microplasticity plays an important role in deformation and failure of ceramics and ceramic composites at stresses even below the Hugoniot elastic limit (HEL) under dynamic loading conditions; see Lankford (1977, 1981), Longy and Cagnoux (1989), Ramesh and Ravichandran (1990), Ravichandran and Chen (1991), Raiser and Clifton (1993), Subhash and Nemat-Nasser (1993) and Subhash and Ravichandran (1993). Rocks and minerals also undergo damage in the form of microcracking under compressive and tensile pulse loading; for example, see Grady (1977) and Rubin and Ahrens (1991). A dominant micromechanism that commonly characterizes damage in brittle or quasi-brittle materials is microcracking which may nucleate either at inhomogeneities such as inclusions and reinforcements or at defects such as microcracks and pores. In the present study, we develop an analytical model for damage evolution in brittle solids under high strain rate loading and provide a quantitative understanding for the observed rate sensitivity in ceramics under compressive loading conditions.

A brief review of compressive failure in ceramic materials is presented in Section 2 and the possible micromechanisms responsible for damage are outlined. In Section 3, theory for damage evolution under biaxial compressive loading is presented. The modeling is based on a sliding crack model proposed by Brace and Bombolakis (1963) and subsequently

† Currently with the Department of Mechanical Engineering and Engineering Mechanics, Michigan Technological University, Houghton, MI 49931, U.S.A.

analyzed in detail by Nemat-Nasser and Horii (1982). Results from this model are used to formulate a constitutive relation on a macroscopic level using the Clapeyron relation. A brief review of the crack growth criteria is also presented in this section. In Section 4, a dynamic crack growth criterion is used to model the response of brittle solids under constant strain rate loading. This corresponds to the condition experienced by a specimen when subjected to uniaxial compressive loading in a split Hopkinson (Kolsky) pressure bar. The predictions are correlated with the observed high strain rate behavior of a hot pressed aluminum nitride (Subhash and Ravichandran, 1993). The physical significance of model parameters and their implications for failure of ceramics are critically examined. Improvements for the model are suggested and conclusions for the current study are presented in Section 5.

2. COMPRESSIVE FAILURE OF CERAMICS

In brittle materials such as rocks, minerals, ceramics and composites, the damage evolution under applied compressive loading is intimately related to microcracking at defects such as pores, inclusions, second phase particles, twin/grain boundary intersections and triple point grain boundary junctions; see for example, Lankford (1977). The compressive strength of ceramic materials has been found to be rate sensitive and the possible mechanisms for this observed rate sensitivity have been discussed by Lankford (1981). It was observed that certain ceramic materials are weakly rate sensitive (hot pressed Al_2O_3) and others are rate insensitive (sintered α-SiC) below a certain critical strain rate, which is typically on the order of 1000 s^{-1}. Above this critical strain rate, it is observed that most ceramic materials exhibit a strong strain rate sensitivity. Compressive failure involves nucleation of tensile microcracks from inhomogeneities or flaws which eventually coalesce and cause axial splitting. However, the mechanisms and thermal activation of these processes vary and could be functions of strain rate. Below the critical strain rate, in hot pressed Al_2O_3 and sintered α-SiC, it has been found that while the microcracks nucleate athermally, their growth process is thermally activated and is a function of the material properties.

In hot pressed ceramics, the tensile cracks can nucleate and grow in a stable manner below the critical strain rate. This could be due to mismatches in elastic compliance between adjacent grains and from the inherently present processing flaws such as the ones at the twin/grain boundary intersections. In such materials, it has been speculated that the strain rate exponent is closely related to the characteristics of the sub-critical crack growth (K_I–v relation); see, for example, Evans (1972). The sub-critical crack growth has also been cited as the reason for observed rate sensitivity of tensile failure in the quasi-static strain rate regime. On the other hand, sintered ceramics are relatively insensitive in their failure strength below the critical strain rate. Stable sub-critical crack growth is not generally found in sintered materials where the initial flaws are typically sharp cornered pores (Lankford, 1977). In such cases, the cracks nucleate athermally and the coalescence occurs instantaneously without any sub-critical crack growth.

Above the critical strain rate, it is found that most ceramic materials, either hot pressed or sintered (irrespective of the processing conditions), exhibit strongly rate sensitive behavior. It has also been found (Lankford, 1981) that the strain rate sensitivity exponent is nearly the same for all ceramics, 0.27 for Al_2O_3 and 0.263 for α-SiC. This has been attributed to the inertia-dominated dynamic crack growth from pre-existing flaws. The crack initiation has been considered to be athermal and once the crack initiates, the rate controlling process is considered to be inertia which is suggested to be independent of material properties. Based on arguments concerning the inertial effects on initiation and propagation of cracks, Grady and Lipkin (1980) showed that the strain rate sensitivity exponent is 1/3 and that this exponent is independent of material properties and thermal activation. It was noted by Lankford (1981) that extrapolating to higher strain rates (shock wave data) using this exponent could possibly explain the high HEL observed for ceramics. The data on hot pressed aluminum nitride (Subhash and Ravichandran, 1993) show that it is weakly rate sensitive in the low strain rate regime and strongly rate sensitive above strain rates of approximately 1000 s^{-1}.

From a mechanics point of view, the situation in hot pressed ceramics is closely related to the problem of sliding microcracks nucleating tensile wing cracks upon reaching a critical stress intensity factor K_{Ic} and then growing in a stable manner in the direction of compression; for example, see Horii and Nemat-Nasser (1986) and Ashby and Hallam (1986). On the other hand, the observations for sintered ceramics can be modeled in terms of cracks nucleating from defects such as pores due to local tension and the subsequent crack growth and coalescence in the direction of applied compression; see Sammis and Ashby (1986). Also, the reason for lack of stable sub-critical crack growth in sintered materials can be understood in terms of their processing and crack initiation process. It has been noted by Lange (1983) that in sintered ceramics, the thermal gradients during sintering could result locally in larger size flaws. Also, the presence of sintering additives in ceramics could result in additional nucleation sites such as low aspect pores at triple junctions and quasi-brittle glassy phases at grain boundaries. If the initiation flaws are low aspect ratio pores, the material has the ability to store large amounts elastic energy, and hence once the flaw initiates at higher stress intensity factor (K_I) (values exceeding K_{Ic}), then the cracks would propagate in an unstable manner. The problem of crack initiation and dynamic propagation from flaws with stress concentrations has been examined by Freund (1977, 1990). The presence of larger flaws in sintered ceramics as observed by Lange (1983) would also promote catastrophic failure upon initiation. These observations would explain the rate insensitivity of sintered materials below the critical strain rate since they will not be able to sustain stable crack growth. During processing of hot pressed ceramics, the lack of sintering additives and thermal gradients, and prevailing high pressures, promote good bonding at particle boundaries, lower porosity and smaller pores; see Lange (1983). The presence of small microflaws would result in sliding upon reaching the critical stress intensity factor at the crack tip and could grow in a stable manner as has been suggested by Nemat-Nasser and Horii (1982) and Ashby and Hallam (1986). In the following section, we will examine the implications of these observations both at quasi-static and high strain rates.

3. DAMAGE EVOLUTION

3.1. *Sliding crack model for tensile cracking under overall compression*

A material element subjected to overall compressive loading is assumed to contain distributed pre-existing microcracks as shown in Fig. 1(a), and the tension cracks are nucleated at the tips of individual microcracks as shown in Fig. 1(b). The problem of crack

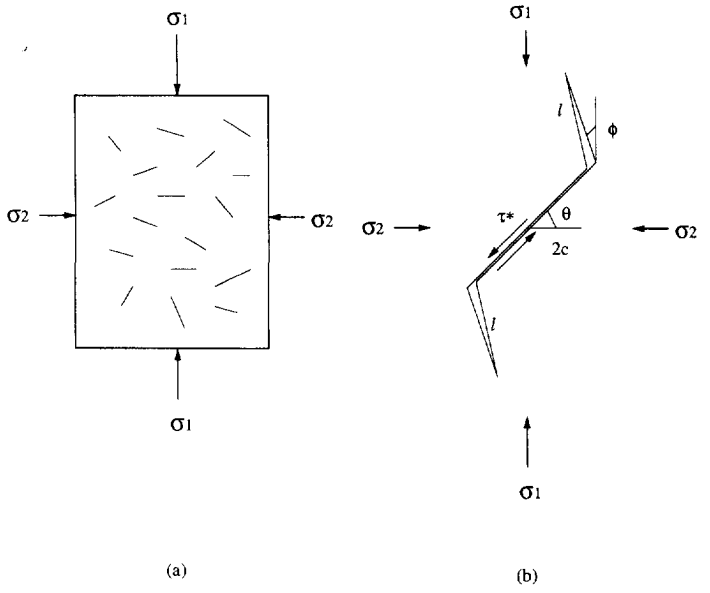

Fig. 1. (a) A schematic of a material element with distributed microcracks subjected to far-field biaxial compression and (b) sliding crack model for individual microcracks.

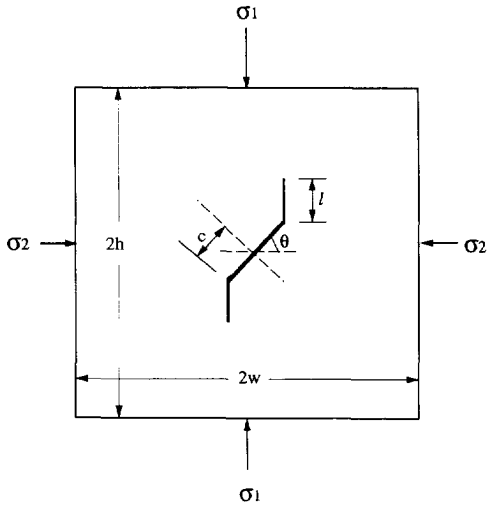

Fig. 2. An idealized unit cell model for sliding crack under applied biaxial compression.

growth under compression has been analyzed extensively by Nemat-Nasser and Horii (1982), Horii and Nemat-Nasser (1986), Ashby and Hallam (1986) and Ashby and Sammis (1990). Earlier analyses of the problem include the ones by McClintock and Walsh (1963) and Moss and Gupta (1982). The tension cracks (wings) are assumed to nucleate and grow so as to maximize the mode I stress intensity factor, K_I. The cracks are assumed to be dilutely distributed and randomly oriented in the material. The unit cell model problem used in the present study of local tension-induced microcracking in brittle solids is shown in Fig. 2 where the cracks grow in the direction of maximum applied compression. Under overall compressive loading, the failure mode depends on the relative magnitude of the principal stresses. In tension, a single dominant flaw grows in an unstable manner and causes catastrophic failure, while in compression a number of microcracks can grow in a stable manner under increasing loads until they interact, coalesce and cause eventual failure.

The pre-existing microcracks are assumed to be of initial length $2c$ and the length of each sigmoidal tension crack is assumed to be l. To simplify the problem, we have replaced the curved wing cracks by straight cracks, i.e. $\phi = 0$ [see Fig. 1(b)], as has been suggested by Ashby and Hallam (1986). This assumption is reasonable since the tensile wing grows to several times the original length of the original sliding crack, i.e. $l \gg c$ and the crack curves only in the initial stages when $l \leqslant c$ which then eventually propagates in the direction of maximum applied compression; also see Vekinis *et al.* (1991). The mode I and mode II stress intensity factors K_I and K_{II} at the tip of each of the tension cracks shown in Fig. 2 under biaxial compressive loading are given by

$$K_I = \frac{2c\tau^* \cos\theta}{\sqrt{[\pi(l+l_*)]}} - \sigma_2\sqrt{(\pi l)} \quad \text{and} \quad K_{II} = \frac{-2c\tau^* \sin\theta}{\sqrt{[\pi(l+l_*)]}}, \tag{1a,b}$$

where τ^* is the shear stress on the pre-existing microcrack that causes sliding,

$$\tau^* = \tfrac{1}{2}(\sigma_1 - \sigma_2)\sin 2\theta - \tau_f, \tag{2}$$

where

$$\tau_f = \tfrac{1}{2}\eta[(\sigma_1 + \sigma_2) + (\sigma_1 - \sigma_2)\cos 2\theta]. \tag{3}$$

The first term in eqn (2) is the resolved shear stress on the crack faces that provides the driving force for sliding and propagation of the tensile cracks. The second term τ_f is the shear traction on the crack faces due to the normal traction caused by the external loading σ_1 and σ_2 applied in the x_1 and x_2 directions, respectively. In our analysis, the compressive stress components are assumed to be positive. The frictional shear stress τ_f on the microcrack

resists sliding. η is the coefficient of friction. The frictional stresses are assumed to be uniform across the faces of the sliding crack. The crack length l_* has been introduced so that when the length of tension crack is extremely small, the stress intensity factors are accurately given by eqn (1). l_* has been estimated (Horii and Nemat-Nasser, 1986) to be $0.27c$. Several other microcrack-induced failures of materials under compression have been proposed, e.g. by Kachanov (1982), Costin (1983, 1987), Ortiz (1985), Krajcinovic (1989) and Myer *et al.* (1992). Most of the above-mentioned models deal with quasi-static failure of brittle materials under compressive loading. Recent investigations by Deng and Nemat-Nasser (1993) and Nemat-Nasser and Deng (1994) deal with damage evolution under dynamic compressive loading conditions and their implications on rate dependence of brittle materials.

The virtual energy release rate G is given by,

$$G = \frac{(\kappa+1)(1+\nu)}{4E}(K_{\mathrm{I}}^2 + K_{\mathrm{II}}^2), \tag{4}$$

where $\kappa = (3-\nu)/(1+\nu)$ for plane stress and $\kappa = (3-4\nu)$ for plane strain. Hence,

$$G(l) = \frac{(\kappa+1)(1+\nu)}{4E}\left[\frac{4c^2(\tau^*)^2}{\pi(l+l_*)} + \sigma_2^2\pi l - 4c\tau^*\sigma_2\cos\theta\sqrt{\left(\frac{l}{(l+l_*)}\right)}\right], \tag{5}$$

where E and ν are the uniaxial Young's modulus and Poisson's ratio, respectively.

3.2. *Quasi-static compressive strength*

The sliding crack models predict that the initiation stress for crack advance in biaxial compression is given by (Nemat-Nasser and Horii, 1982; Ashby and Hallam, 1986),

$$\sigma_1 = \frac{[(1+\eta^2)^{1/2}+\eta]}{[(1+\eta^2)^{1/2}-\eta]}\sigma_2 + \frac{\sqrt{3}}{[(1+\eta^2)^{1/2}-\eta]}\frac{K_{\mathrm{Ic}}}{\sqrt{(\pi c)}}. \tag{6}$$

Equation (6) highlights the parameters that influence the compressive strength of brittle materials such as ceramics. Smaller initial flaw size (microcrack) and higher fracture toughness (critical stress intensity factor, K_{Ic}) would mean higher compressive strength for the material. For uniaxial compressive loading, eqn (6) can be written as (Ashby and Sammis, 1990),

$$\sigma_0 = \frac{\sqrt{3}}{[(1+\eta^2)^{1/2}-\eta]}\frac{K_{\mathrm{Ic}}}{\sqrt{(\pi c)}}, \tag{7}$$

where σ_0 is viewed as the quasi-static compressive strength (at extremely low strain rates) of the material under uniaxial compression. The fracture toughness K_{Ic} is a material property that has been determined from independent measurements, c is the average initial flaw size (related to processing) from which the tension cracks nucleate and η, the coefficient of friction, can either be measured or could be obtained from fitting parameters to the experimental data. *In situ* observations in ceramics by Vekinis *et al.* (1991) suggest that when the axial stress exceeds σ_0, these nucleated cracks grow parallel to the compression axis in a stable manner, and avoid each other until ultimately they coalesce, causing failure.

3.3. *Constitutive behavior*

The constitutive behavior of brittle materials subjected to compressive loading has been studied by Moss and Gupta (1982), Nemat-Nasser and Obata (1988) and Myer *et al.* (1992) under quasi-static loading conditions, and under stress pulse loading by Deng and Nemat-Nasser (1993). In the two-dimensional principal axis setting (see Figs 1 and 2) the stress $\boldsymbol{\sigma}$ and strain $\boldsymbol{\varepsilon}$ tensors are represented by the following 2×1 arrays,

$$\boldsymbol{\sigma} = \begin{pmatrix} \sigma_1 \\ \sigma_2 \end{pmatrix} \quad \text{and} \quad \boldsymbol{\varepsilon} = \begin{pmatrix} \varepsilon_1 \\ \varepsilon_2 \end{pmatrix}. \tag{8}$$

The total strain tensor $\boldsymbol{\varepsilon}$ can be represented by an additive split,

$$\boldsymbol{\varepsilon} = \boldsymbol{\varepsilon}^{\mathrm{e}} + \boldsymbol{\varepsilon}^{\mathrm{d}}, \tag{9}$$

where $\boldsymbol{\varepsilon}^{\mathrm{e}}$ is the strain tensor associated with the solid prior to damage accumulation and is related to the stress tensor $\boldsymbol{\sigma}$ through the compliance tensor $\mathbf{D}$,

$$\boldsymbol{\varepsilon}^{\mathrm{e}} = \mathbf{D}\boldsymbol{\sigma}. \tag{10}$$

The compliance tensor $\mathbf{D}$ can be written in two dimensions as a 2×2 matrix,

$$\mathbf{D} = \frac{(\kappa+1)(1+\nu)}{4E} \begin{bmatrix} 1 & \dfrac{\kappa-3}{\kappa+1} \\ \dfrac{\kappa-3}{\kappa+1} & 1 \end{bmatrix}. \tag{11}$$

In the case of plane strain $\varepsilon_3 = 0$ and in the case of plane stress, $\sigma_3 = 0$. For plane stress,

$$\varepsilon_3^{\mathrm{e}} = -\frac{\nu}{E}(\sigma_1 + \sigma_2). \tag{12}$$

The elastic part of the volumetric strain Θ^{e} is given by,

$$\Theta^{\mathrm{e}} = \frac{(1-2\nu)}{3E}(\sigma_1 + \sigma_2 + \sigma_3). \tag{13}$$

$\boldsymbol{\varepsilon}^{\mathrm{d}}$ is the damage strain for the material element under consideration due to the presence of initial microcracks and the subsequent growth of sigmoidal tensile cracks. The damage strain tensor has been evaluated by Nemat-Nasser and Obata (1988) by making use of the cavity strain approach for individual microcracks and summing them over all possible orientations. In our present modeling we adopt the energy approach suggested by Palmer and Rice (1973). In this approach, we make use of the global energy balance to evaluate the additional strains induced by the tensile cracks and sliding of the microcrack. We utilize the Clapeyron relation,

$$2U_{\mathrm{e}} = W_{\mathrm{i}} - W_{\mathrm{f}}, \tag{14}$$

where U_{e} is the elastic strain energy dissipated by the growth of the tensile cracks, W_{i} is the increase in elastic strain energy of the body due to the introduction of the crack and W_{f} is the frictional dissipation due to the sliding of the crack surfaces. The strain energy dissipated at each crack tip can be evaluated by making use of the well-known relation,

$$G = \left.\frac{\partial U_{\mathrm{e}}}{\partial l}\right|_{P}, \tag{15}$$

where U_{e} is the strain energy associated with each crack tip, l is the crack length and P is used to denote fixed load conditions. By integrating G in eqn (5) with respect to the crack length l while holding the applied loads constant, i.e. the far field stress components σ_1 and σ_2, we obtain, U_{e} (equal to $2U_{\mathrm{e}}$, since there are two crack tips),

$$U_e(l) = \frac{2c^2(\kappa+1)(1+\nu)}{\pi E}\left\{(\tau^*)^2 \ln\left(1+\frac{l}{l_*}\right)+\tfrac{1}{8}\sigma_2^2\left(\frac{\pi l}{c}\right)^2\right.$$

$$\left.-\pi\tau^*\sigma_2\cos\theta\left(\frac{l_*}{c}\right)\left[\sqrt{\left(\frac{l}{l_*}\left(1+\frac{l}{l_*}\right)\right)}-\ln\left(\sqrt{\frac{l}{l_*}}+\sqrt{\left(1+\frac{l}{l_*}\right)}\right)\right]\right\}. \quad (16)$$

For our modeling purposes, we assume that the initial state is characterized by the solid with initial microcracks under biaxial loading and the constitutive relation is given by eqn (10). The strain due to damage is assumed solely due to the sliding of the microcracks and the growth of tensile wing cracks. The global strain increments due to damage is computed using the Clapeyron relation (14). The strain increments in ε_1 and ε_2 due to each crack are denoted by $\Delta\varepsilon_1$ and $\Delta\varepsilon_2$. The total sliding displacement on the crack faces is given by δ and is normalized by the initial microcrack length $2c$. Based on the linearity of the problem under consideration, the strain increments $\Delta\varepsilon_1$ and $\Delta\varepsilon_2$ are assumed to be linearly dependent on the biaxial stress components σ_1 and σ_2,

$$\begin{pmatrix}\Delta\varepsilon_1\\ \Delta\varepsilon_2\end{pmatrix} = \begin{bmatrix}S_{11} & S_{12}\\ S_{21} & S_{22}\end{bmatrix}\begin{pmatrix}\sigma_1\\ \sigma_2\end{pmatrix}, \quad (17)$$

where $S_{\alpha\beta}$ are constants. From the symmetry of the modulus tensor, we have $S_{21} = S_{12}$. Under fixed loading conditions, the work W_1 done by the applied loads, i.e. σ_1 and σ_2, on the additional displacements is

$$W_1 = 4wh(\sigma_1\Delta\varepsilon_1 + \sigma_2\Delta\varepsilon_2), \quad (18)$$

and the frictional dissipation W_f can be written as,

$$W_f = 2c\tau_f\delta, \quad (19)$$

where $4wh$ is the area of the unit cell in which the crack is present (see Fig. 2) and δ is the sliding displacement along the crack faces. The sliding displacement δ is computed from the stress intensity factor at the tension crack tip due to sliding K_I^s (Nemat-Nasser and Obata, 1988),

$$K_I^s = \frac{2E}{(\kappa+1)(1+\nu)}\frac{\delta\cos\theta}{\sqrt{[2\pi(l+l_{**})]}} - \sigma_2\sqrt{\left(\frac{\pi l}{2}\right)}, \quad (20)$$

where $l_{**} = 0.083c$ which assures the correct value for the stress intensity factor as the length of the tension crack l becomes vanishingly small in eqn (20). The stress intensity due to sliding should be the same as the one due to the applied loading given by eqn (1a). The sliding displacement is written in terms of the stress intensity factor K_I and hence the applied biaxial loading components by equating eqns (1a) and (20). The sliding displacement δ can be written as

$$\delta = \frac{c(\kappa+1)(1+\nu)}{(\sqrt{2})E}\left\{2\tau^*\sqrt{\left(\frac{l+l_{**}}{l+l_*}\right)}-\frac{((\sqrt{2})-1)\sigma_2}{(\sqrt{2})\cos\theta}\frac{\pi l_{**}}{c}\sqrt{\left(\frac{l}{l_{**}}\left(1+\frac{l}{l_{**}}\right)\right)}\right\}. \quad (21)$$

The work done by the applied loads on the additional displacements due to the growth of the tensile wing crack, W_1 [see eqn (18)] and the frictional dissipation, W_f [see eqn (19)] can now be written as

$$W_1 = 4wh(S_{11}\sigma_1^2 + S_{22}\sigma_2^2 + 2S_{12}\sigma_1\sigma_2), \tag{22}$$

$$W_f = \frac{(\sqrt{2})c^2\eta(\kappa+1)(1+\nu)}{E}\left\{2(\tau^*\sigma_1\cos^2\theta + \tau^*\sigma_2\sin^2\theta)\sqrt{\left(\frac{l+l_{**}}{l+l_*}\right)}\right.$$
$$\left. - \frac{((\sqrt{2})-1)(\sigma_1\sigma_2\cos\theta + \sigma_2^2\tan\theta\sin\theta)}{\sqrt{2}}\frac{\pi l_{**}}{c}\sqrt{\left(\frac{l}{l_{**}}\left(1+\frac{l}{l_{**}}\right)\right)}\right\}. \tag{23}$$

By making use of the Clapeyron relation (14) and eqn (22) and (23), we can solve for the constants S_{11}, S_{22} and S_{12} in eqn (22), by comparing the coefficients of the quadratic terms,

$$S_{11} = \frac{4c^2(\kappa+1)(1+\nu)}{EA_c}\left\{\frac{(\sin\theta-\eta\cos\theta)^2\cos^2\theta}{\pi}\ln\left(1+\frac{l}{l_*}\right)\right.$$
$$\left. + \frac{\eta(\sin\theta-\eta\cos\theta)\cos^3\theta}{\sqrt{2}}\sqrt{\left(\frac{l+l_{**}}{l+l_*}\right)}\right\}, \tag{24a}$$

$$S_{22} = \frac{4c^2(\kappa+1)(1+\nu)}{EA_c}\left\{\frac{(\cos\theta+\eta\sin\theta)^2\sin^2\theta}{\pi}\ln\left(1+\frac{l}{l_*}\right) + \frac{1}{8\pi}\left(\frac{\pi l}{c}\right)^2\right.$$
$$+ \frac{(\cos\theta+\eta\sin\theta)\sin 2\theta}{2}\left(\frac{l_*}{c}\right)\left[\sqrt{\left(\frac{l}{l_*}\left(1+\frac{l}{l_*}\right)\right)} - \ln\left(\sqrt{\frac{l}{l_*}} + \sqrt{\left(1+\frac{l}{l_*}\right)}\right)\right]$$
$$- \frac{\eta(\cos\theta+\eta\sin\theta)\sin^3\theta}{\sqrt{2}}\sqrt{\left(\frac{l+l_{**}}{l+l_*}\right)} - \frac{((\sqrt{2})-1)\eta\sin\theta\tan\theta}{4}$$
$$\left.\times\left(\frac{\pi l_{**}}{c}\right)\sqrt{\left(\frac{l}{l_{**}}\left(1+\frac{l}{l_{**}}\right)\right)}\right\}, \tag{24b}$$

$$S_{12} = -\frac{4c^2(\kappa+1)(1+\nu)}{EA_c}\left\{\frac{[(1-\eta^2)\sin 2\theta - 2\eta\cos 2\theta]\sin 2\theta}{4\pi}\ln\left(1+\frac{l}{l_*}\right)\right.$$
$$+ \frac{(\sin\theta-\eta\cos\theta)\cos^2\theta}{2}\left(\frac{l_*}{c}\right)\left[\sqrt{\left(\frac{l}{l_*}\left(1+\frac{l}{l_*}\right)\right)} - \ln\left(\sqrt{\frac{l}{l_*}} + \sqrt{\left(1+\frac{l}{l_*}\right)}\right)\right]$$
$$+ \frac{\eta(\cos 2\theta+\eta\sin 2\theta)\sin 2\theta}{4\sqrt{2}}\sqrt{\left(\frac{l+l_{**}}{l+l_*}\right)} + \frac{((\sqrt{2})-1)\eta\cos\theta}{8}$$
$$\left.\times\left(\frac{\pi l_{**}}{c}\right)\sqrt{\left(\frac{l}{l_{**}}\left(1+\frac{l}{l_{**}}\right)\right)}\right\}, \tag{24c}$$

where A_c is the area of the unit cell which in our case is $4wh$ (see Fig. 2). The strain increments which are of interest to us, namely $\Delta\varepsilon_1$ and $\Delta\varepsilon_2$ due to the sliding and growth of a single crack, can now be evaluated using eqns (17) and (24a–c). The out of plane strain increment $\Delta\varepsilon_3$ due to crack sliding and growth is zero for two-dimensional problems. The incremental volumetric strain $\Delta\Theta$ due to crack growth and sliding for a single crack is given by,

$$\Delta\Theta = \Delta\varepsilon_1 + \Delta\varepsilon_2. \tag{25}$$

Assuming no interaction between the cracks, i.e. they are thinly distributed, the overall damage strain tensor ε^{d} [see eqn (9)] can be written for the distribution of microcracks $\hat{N}(\theta)$ in the solid as

$$\varepsilon_\alpha^{\mathrm{d}}(\theta) = \int_{\theta_s}^{\pi/2} \hat{N}(\theta)\Delta\varepsilon_\alpha \,\mathrm{d}\theta, \quad \alpha = 1, 2. \tag{26}$$

In the above integral, note that the lower limit is θ_s which is defined such that $\tau^* < 0$ for $\theta \leqslant \theta_s$ and $\tau^* > 0$ for $\theta > \theta_s$. The angle θ_s can be determined from solving eqn (3) by setting $\tau^* = 0$. The angle θ_s has been introduced to account for the fact that the initial microcracks with orientations $\theta \leqslant \theta_s$ will remain closed and will not undergo sliding or growth since $\tau^* < 0$ and thus do not contribute to the overall strain due to damage accumulation. The pre-existing microcracks are assumed to be randomly oriented which implies $\hat{N}(\theta) = 2\hat{N}/\pi$, where $\hat{N}$ is the total number of pre-existing microcracks in the solid. The strain components due to cumulative damage are given by

$$\varepsilon_\alpha = \varepsilon_\alpha^{\mathrm{e}} + \varepsilon_\alpha^{\mathrm{d}} = \varepsilon_\alpha^{\mathrm{e}} + \frac{2\hat{N}}{(\pi - 2\theta_s)} \int_{\theta_s}^{\pi/2} \Delta\varepsilon_\alpha(\theta)\,\mathrm{d}\theta. \tag{27}$$

The integral in eqn (27) can be evaluated explicitly by integrating expressions for $S_{\alpha\beta}$ in eqn (24) with respect to θ. The areal density of initial microcracks is defined by the parameter f_0 which is related to the initial flaw size c and N, the number of microcracks per unit area,

$$f_0 = Nc^2. \tag{28}$$

The constitutive model can now be constructed using eqns (10)–(13) and (26)–(28) for brittle microcracking solids subjected to biaxial compressive loading.

3.4. *Uniaxial stress deformation*

For uniaxial compressive loading, i.e. $\sigma_1 = \sigma$ and $\sigma_2 = 0$, the state of deformation is assumed to be in plane stress, i.e. $\sigma_3 = 0$. The critical sliding angle θ_s can be written as [see eqn (3)]

$$\theta_s = \arctan(\eta), \tag{29}$$

and note that $0 \leqslant \theta_s \leqslant \pi/4$ for the coefficients of friction in the range $0 \leqslant \eta \leqslant 1$. The expressions for the average shear stress on each crack, the stress intensity factors and the energy release rate at each of the tensile crack tips is obtained by integrating over all possible orientations for the sliding cracks, i.e. $\theta_s \leqslant \theta \leqslant \pi/2$.

$$\tau^* = \frac{\sigma}{2(\pi - 2\theta_s)}[1 + \cos 2\theta_s - \eta((\pi - 2\theta_s) + \eta \sin 2\theta_s)], \tag{30}$$

$$K_{\mathrm{I}} = \frac{4c\sigma}{3(\pi - 2\theta_s)} \sqrt{\left(\frac{1}{\pi(l + l_*)}\right)} (\cos^3\theta_s - \eta\{2 - 3\sin\theta_s + \sin^3\theta_s\}) \tag{31a}$$

and

$$K_{\mathrm{II}} = -\frac{4\sigma c}{3(\pi - 2\theta_s)} \sqrt{\left(\frac{1}{\pi(l + l_*)}\right)} (1 - \sin^3\theta_s - \eta\cos^3\theta_s) \tag{31b}$$

$$G = \frac{1}{E}\frac{\sigma^2 c^2\{2(\pi-2\theta_s)(1+3\eta^2)+(1-\eta^2)\sin 4\theta_s - 16\eta\cos^4\theta_s - 8\eta^2\sin 2\theta_s\}}{4(\pi-2\theta_s)\pi(l+l_*)}. \tag{32}$$

Now the constitutive relations reduce to the following form for uniaxial stress:

$$\varepsilon_1 = \frac{\sigma}{E} + \frac{\sigma}{E} f_0 \left\{ p_1 \ln\left(1+\frac{l}{l_*}\right) + p_2 \sqrt{\left(\frac{l+l_{**}}{l+l_*}\right)} \right\}, \tag{33a}$$

$$\varepsilon_2 = -\frac{\nu\sigma}{E} + \frac{\sigma}{E} f_0 \left\{ q_1 \ln\left(1+\frac{l}{l_*}\right) + q_2\left(\frac{l_*}{c}\right)\left[\sqrt{\left(\frac{l}{l_*}\left(1+\frac{l}{l_*}\right)\right)} - \ln\left(\sqrt{\frac{l}{l_*}} + \sqrt{\left(1+\frac{l}{l_*}\right)}\right)\right] + q_3\sqrt{\left(\frac{l+l_{**}}{l+l_*}\right)} + q_4\left(\frac{\pi l_{**}}{c}\right)\sqrt{\left(\frac{l}{l_{**}}\left(1+\frac{l}{l_{**}}\right)\right)} \right\}, \tag{33b}$$

$$\varepsilon_3 = -\frac{\nu\sigma}{E}. \tag{33c}$$

All other strain components are zero. The constants p_1, p_2, q_1, q_2, q_3 and q_4 are functions of the friction coefficient η and are given in the Appendix. The volumetric strain Θ is given by,

$$\Theta = \varepsilon_1 + \varepsilon_2 + \varepsilon_3. \tag{34}$$

Since we are interested in predicting the failure or the critical strength σ_c of the material in uniaxial compression, with $\varepsilon_1 = \varepsilon$, we can rewrite eqn (33a) as

$$\sigma = \frac{E}{\left\{1 + f_0 p_1 \ln\left(\frac{l}{l_*}+1\right) + f_0 p_2\sqrt{\left(\frac{l+l_{**}}{l+l_*}\right)}\right\}}\varepsilon. \tag{35}$$

Equation (35) can also be expressed in the familiar form $\sigma = \bar{E}\varepsilon$, where $\bar{E}$ is the "effective modulus" [e.g. Budiansky and O'Connell (1976)] for a microcracking solid under uniaxial compression and is related to the modulus E of the undamaged material by,

$$\frac{\bar{E}}{E} = \left\{1 + f_0 p_1 \ln\left(\frac{l}{l_*}+1\right) + f_0 p_2\sqrt{\left(\frac{l+l_{**}}{l+l_*}\right)}\right\}^{-1}. \tag{36}$$

The first term in eqn (36) with coefficient p_1 corresponds to the change in the moduli due to axial crack growth, and the second term with coefficient p_2 corresponds to the change in moduli due to the sliding of microcracks. In general the first term is positive, resulting in degradation of the moduli, and the second term in general is negative, resulting in enhancing the moduli. However, the coefficient p_1 is an order of magnitude larger than the coefficient p_2 (see the Appendix) and the quantity within the square root in the second term is of the order unity for any appreciable crack growth. In general, for engineering ceramics, there is no degradation in elastic moduli due to crack growth and sliding, and hence macroscopically the response would nearly be that of a perfectly linearly elastic solid. These comments also apply to the axial stress versus transverse strain response of the solid. Hence, the volumetric strain Θ (34) is primarily due to the elastic compressibility (13) of the material rather than dilatancy introduced by the sliding and the growth of microcracks. Equations (33a–c) provide the stress–strain relations for a microcracking solid under far-field applied uniaxial compression in terms of the applied stress σ and the average crack

length l. In order to obtain the constitutive behavior of a material, knowledge of the crack growth is required.

3.5. *Crack growth criteria*

The most commonly used fracture criterion for brittle solids such as ceramics under quasi-static conditions is the constant stress-intensity factor criterion which is formally written as

$$K_I(l) = K_{Ic}. \tag{37}$$

Under quasi-static conditions this is equivalent to assuming the Griffith or constant energy release rate criterion, i.e. $G = 2\gamma$, where γ is the surface energy of the solid per unit area. However, if the crack growth rates were to become appreciable relative to the Rayleigh wave speed c_R in the material, then this equivalence is not valid. For linearly elastic solids, the Rayleigh wave speed c_R is the theoretical limit of crack propagation speed; see, for example, Freund (1990).

Evans (1972) and others have observed stable crack growth in ceramic materials under quasi-static loading conditions. They have proposed the following power law relationship for the crack growth velocity, v,

$$v = AK_I^n, \tag{38}$$

where A is a material constant and n is an exponent which is around 50 for hot pressed ceramics. This provides yet another criterion for crack growth in ceramics. For quasi-static deformation, eqns (37) and (38) appear to be the most appropriate crack growth criteria.

At high loading rates, the crack growth rates become appreciable and we need to apply the concepts of dynamic fracture mechanics. There are varied fracture criteria which are used to study dynamic failure of brittle solids. For an excellent review of these criteria, see Freund (1990). We briefly discuss some of the most commonly used criteria for brittle solids; see, for example, Ravichandran and Clifton (1989).

For dynamic crack growth, the stress intensity factor of a growing crack can be related to the crack velocity,

$$\frac{K_{Ic}}{K_I^d(l, t)} \approx \left(1 - \frac{v}{c_R}\right)\left(1 - \frac{v}{c_d}\right)^{-1/2}, \tag{39}$$

where K_I^d is the stress intensity factor for the stationary crack with current length l and c_d is the dilatational (longitudinal) wave speed in the material.

The energy release rate of a dynamically growing crack can also be related to its velocity,

$$\frac{G_c}{G^d(l, t)} \approx 1 - \frac{v}{c_R}, \tag{40}$$

where G_c is the energy release rate required for sustaining crack propagation and $G^d(l, t)$ is the virtual energy release rate for the stationary crack of current length l.

The relationship between the crack speed and applied loading can be written in the following general form,

$$\frac{G_c}{G^d(l, t)} = \left(1 - \frac{v}{v_m}\right)^{\gamma}, \tag{41}$$

where γ is a fitting parameter which characterizes the toughness–crack velocity relation and v_m is the maximum terminal velocity for a dynamically propagating crack. This form is

particularly useful in fitting experimental data, and in most materials the maximum speed for crack propagation has been observed to be only of the order of 0.3–0.5 of the Rayleigh wave speed c_R. For $\gamma = 1$ and $v_m = c_R$ eqn (41) reduces to the special case of the constant energy release rate criterion given by eqn (40).

The right-hand sides of eqns (39) and (40) are universal functions of crack speed v and are independent of the loading; see Freund (1990). The choice of a particular criterion for crack growth is based on observed material behavior. The uniqueness of the K_I–v relationship for rapid crack propagation has been discussed in detail by Dally *et al.* (1985). Relatively little is known regarding the dynamic fracture characteristics of brittle materials such as ceramics; see Duffy *et al.* (1988, 1989), Yang and Kobayashi (1990), Suresh *et al.* (1990) and Deobald and Kobayashi (1992). However, there is evidence that the dynamic fracture toughness of a dynamically growing crack in monolithic ceramics may be decreasing with increasing velocity; see Kobayashi *et al.* (1983) and Yang and Kobayashi (1990). For modeling purposes, we assume the following relation for the energy release rate G_c for propagation

$$\frac{G_c}{G_0} = h(l, \dot{l}), \tag{42}$$

where h is a function to be fitted from experimental data and G_0 is the critical energy release rate at initiation.

3.6. *Failure criteria*

A physically acceptable failure criterion for which the material element loses its capability to carry or transmit loads is when the damage reaches a critical value f_c. The critical density of damage f_c is expressed as [see eqn (28)]

$$f_c = N l_c^2, \tag{43}$$

where l_c is a critical length for the tension crack when the coalescence occurs with neighboring tension cracks.

4. CONSTITUTIVE MODELING

We illustrate the application of the constitutive model developed for plane stress in the previous section for constant strain rate deformation under uniaxial compressive loading. This can then be used to model the experimental data obtained from split Hopkinson (Kolsky) pressure bar experiments.

4.1. *Constant strain rate deformation*

When a material element is subjected to a constant strain rate $\dot{\varepsilon}_0$, the strain ε can be written as,

$$\varepsilon = \dot{\varepsilon}_0 t, \tag{44}$$

and stress σ in the material element can be expressed as a function of the reduced modulus $\bar{E}$ [see eqn (36)],

$$\sigma = \bar{E}\dot{\varepsilon}_0 t. \tag{45}$$

The microcracks are assumed to initiate when the far-field applied compressive stress reaches the quasi-static compressive strength σ_0 which is assumed to be athermal (see Section 2). In other words, when the applied stress level reaches the quasi-static compressive strength then the crack-tip stress intensity factor attains its critical value K_{Ic}, which is assumed to be rate independent and athermal in the present study.

The following non-dimensional variables for stress Σ, time T and length L are used:

$$\Sigma = \sigma(t)/\sigma_0, \quad T = t/t_0 \quad \text{and} \quad L = l/l_0, \tag{46}$$

where stress σ is normalized with respect to the quasi-static compressive strength σ_0, time t is normalized with respect to t_0 and crack length l is normalized with respect to a characteristic length $l_0 = v_m t_0$. t_0 is the time taken from time $t = 0$ for the material element to reach the stress level σ_0 which can be determined from eqn (45).

Making use of eqns (36) and (45), the stress in the material element can be written as,

$$\Sigma(T, L) = \frac{T[1 + p_2\sqrt{(1-\chi)}]}{\left(1 + p_1 \ln\left(\frac{l}{l_*} + 1\right) + p_2\sqrt{\left(1 - \frac{\chi}{(l/l_*)+1}\right)}\right)}, \tag{47}$$

where χ is a constant given by $(l_* - l_{**})/l_*$ (see Section 3). Using eqn (47) and the fracture criteria discussed in Section 3.5, one can study the effect of strain rate on the deformation and failure response of a material.

4.2. *High strain rate behavior*

Using eqns (41), (42) and (45), the relationship between the crack speed and the applied loading can be written in the form

$$\frac{1}{v_m}\frac{dl}{dt} = 1 - h^{1/\gamma}\left(\frac{\sigma_0}{\sigma}\right)^{2/\gamma}\left(\frac{l}{c}\right)^{1/\gamma}. \tag{48}$$

Equation (48) is an ordinary differential equation which relates the crack growth rate to the applied loading. This equation can be integrated to obtain crack length as a function of the applied stress σ. Inspection of eqn (48) suggests that the crack would cease to grow unless h is a monotonically decreasing function of the crack length l. Motivated by the limited experimental data available (Kobayashi *et al.*, 1983; Yang and Kobayashi, 1990) on ceramics, the following form for the function h is postulated:

$$h(l, \dot{l}) = \left(\frac{c}{l}\right) + \left(\frac{c}{l_0}\right). \tag{49}$$

Making use of eqns (47)–(49), the equation of motion for a growing microcrack in a material element subjected to constant strain rate uniaxial compressive loading can be written as

$$\left(\frac{dL}{dT}\right) = 1 - \left(\frac{1}{T}\right)^{2/\gamma} \frac{\left(1 + p_1 \ln\left(\frac{l}{l_*} + 1\right) + p_2\sqrt{\left(1 - \frac{\chi}{(l/l_*)+1}\right)}\right)^{2/\gamma}}{[1 + p_2\sqrt{(1-\chi)}]^{2/\gamma}} (L+1)^{1/\gamma}. \tag{50}$$

Equation (50) is integrated numerically using the fourth-order Runge–Kutta method with the initial condition, $L = 0$ at $T = 1$, to obtain the crack length l as a function of time t.

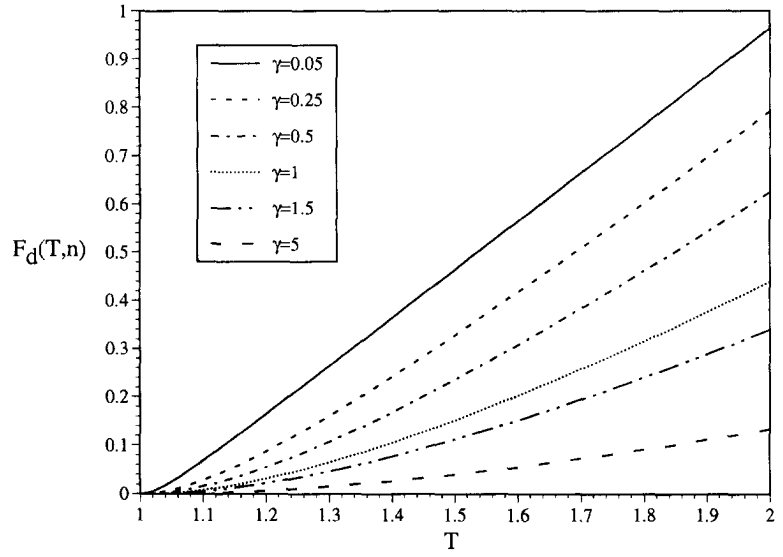

Fig. 3. Plot of the dynamic crack growth function $F_d(T, \gamma)$ versus normalized time T for $\gamma = 0.05$, 0.25, 0.5, 1.0, 1.5 and 5 for initial microcrack density $f_0 = 10^{-3}$ and coefficient of friction $\eta = 0.6$.

The integral of the right-hand side, F_d, is plotted against the normalized time T in Fig. 3 for different values of γ and for $\eta = 0.6$ and $f_0 = 10^{-3}$ (0.1% porosity), which are typical values for engineering ceramics. The relation between crack length l and this universal function F_d can be written as

$$\frac{l(t)}{l_0} = F_d(T, \gamma). \tag{51}$$

The dynamic fracture toughness K_{Id} is plotted as a function of the crack velocity v for $\gamma = 1$ in Fig. 4. The dynamic fracture toughness is normalized with respect to the initiation toughness K_{Ic} and the velocity is normalized with respect to the terminal velocity v_m. The K_I–v relation is a monotonically decreasing function which has been observed experimentally in brittle material systems.

The function F_d on the left-hand side in eqn (51) can be evaluated for a given set of uniaxial compression experiments at failure by invoking the failure criterion eqn (43), i.e.

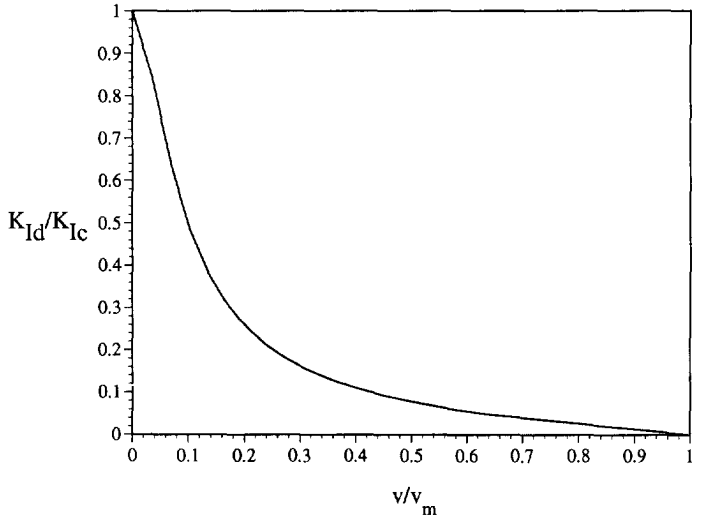

Fig. 4. Normalized dynamic fracture toughness (K_{Id}/K_{Ic}) as a function of normalized crack velocity (v/v_m) for $\gamma = 1$.

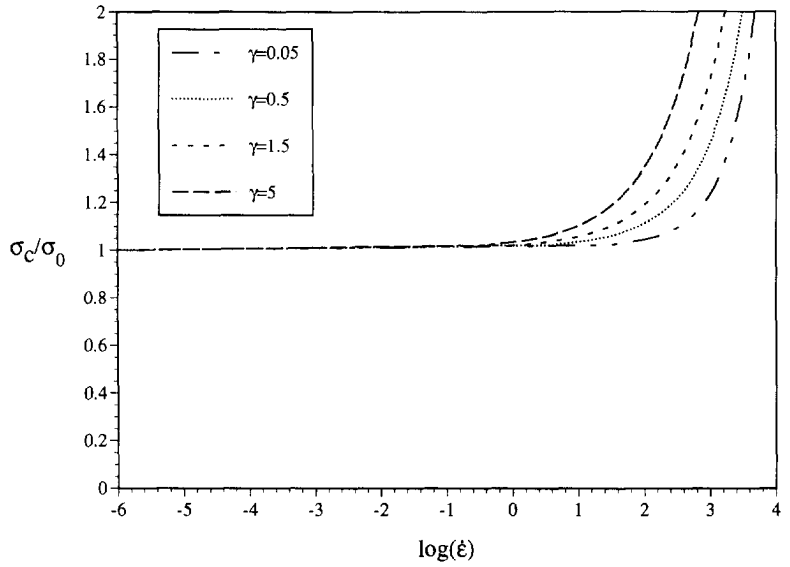

Fig. 5. Compressive strength versus strain rate of a brittle microcracking solid for toughening parameters $\gamma = 0.05, 0.5, 1.5$ and 5 for initial microcrack density $f_0 = 10^{-3}$ and coefficient of friction $\eta = 0.6$.

failure occurs when the average crack length l reaches its critical length l_c and the corresponding failure time is denoted by t_c,

$$\frac{l_c}{l_0} = F_d\left(\frac{t_c}{t_0}, \gamma\right). \tag{52}$$

Knowing the failure time t_c and the corresponding t_0, one can predict the failure strength using eqn (45) [$\sigma_c(= \bar{E}\dot{\varepsilon}_0 t_c)$] of the material for different strain rates. Our present analysis indicates that the most important factor that governs the rate-dependent behavior of ceramics appears to be the dynamic crack growth behavior in them. By making use of eqns (47) and (52) and assuming $l_c/v_m = 2$ μs and quasi-static failure strain to be 0.01, normalized compressive strength is plotted in Fig. 5 as a function of strain rate for $\gamma = 0.05$, 0.5, 1.5 and 5 with $f_0 = 10^{-3}$ and $\eta = 0.6$. It is interesting to note that the material with higher γ becomes highly rate sensitive at lower strain rates than for smaller values of γ. It has been observed that for engineering ceramics, the material is strongly rate sensitive beyond a critical strain rate (Lankford, 1981) and the compressive strength σ_c can be written in the following power law form,

$$\sigma_c \propto \dot{\varepsilon}^n, \tag{53}$$

where n is the strain rate hardening exponent. The strain rate hardening exponent n is plotted in Fig. 6 as a function of the toughening exponent γ for parameters used in Fig. 5. It is clear that the strain rate hardening exponent n decreases monotonically with increasing γ. For illustrative purposes, by making use of eqn (47), the axial stress versus axial strain is plotted in Fig. 7 for strain rates of 500, 1000 and 2000 s^{-1}. It is evident that there is very little or no degradation of the elastic moduli until failure and this is expected to be true for most engineering ceramics. For all practical purposes, these materials can be assumed to be linearly elastic up to failure in uniaxial compression.

4.3. *Transition strain rate*

A critical strain rate at which transition to strongly rate sensitive behavior occurs for microcracking solids is proposed in terms of their material properties

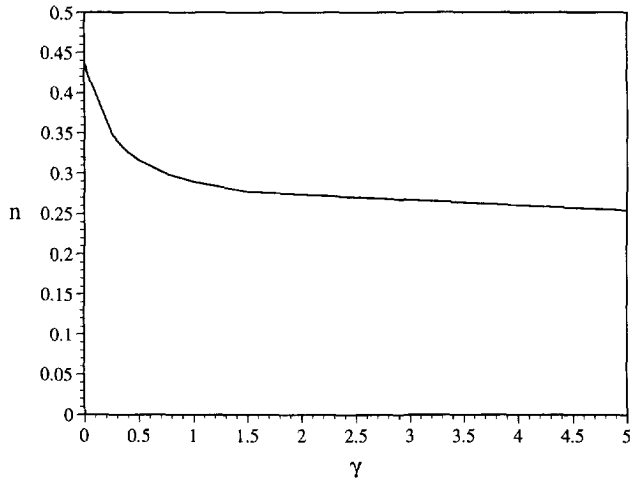

Fig. 6. Strain rate hardening exponent n as a function of the toughening parameter γ for initial microcrack density $f_0 = 10^{-3}$ and coefficient of friction $\eta = 0.6$.

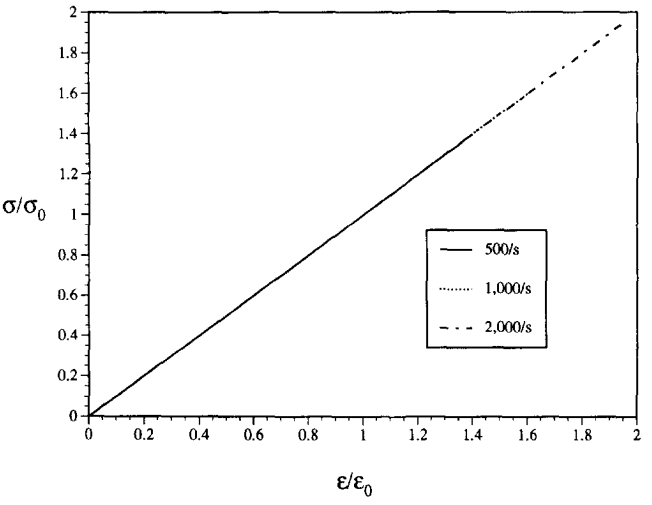

Fig. 7. Axial stress versus axial strain at strain rates $\dot{\varepsilon} = 500$, 1000 and 2000 s^{-1} for initial microcrack density $f_0 = 10^{-3}$, coefficient of friction $\eta = 0.6$ and toughening exponent $\gamma = 1$.

$$\dot{\varepsilon}_* = \frac{\sigma_0}{E}\frac{c_*}{l_s}, \tag{54}$$

where c_* is a characteristic speed and l_s is the length of the material element under consideration, e.g. specimen length in a split Hopkinson (Kolsky) pressure bar experiment. It has been noted that inertial effects become significant when the crack velocities reach about 0.2 of the shear wave speed c_s, which we choose to be c_*. Lankford (1981) had proposed an expression similar to eqn (54) with the radius of the specimen in place of the specimen length l_s and the shear wave speed c_s replacing the critical velocity c_*. For most engineering ceramics E/σ_0 is between 100 and 150 and c_* is in the range 1200–1400 m s^{-1}. For a typical specimen length of 8 mm, the critical strain rate at which the transition occurs is between 1000 and 1200 s^{-1}. This appears to be consistent with most experimental observations on uniaxial compressive behavior of ceramics using a split Hopkinson (Kolsky) pressure bar (Lankford, 1981; Subhash and Ravichandran, 1993).

4.4. *Modeling uniaxial compressive behavior of aluminum nitride*

Both quasi-static and high strain rate experiments have been performed recently on a hot pressed aluminum nitride; see Subhash and Ravichandran (1993). The quasi-static

experiments were conducted in the range 10^{-6}–10^{-2} s^{-1} using a materials testing system (MTS), and the high strain rate experiments were performed in the range 250–2300 s^{-1} using a split Hopkinson (pressure) bar. The material is relatively rate insensitive in the low strain rate regime while at high strain rates (>1000 s^{-1}), the material becomes strongly rate sensitive. The length of the specimens that were used in the experiments was 7.62 mm. The quasi-static compressive strength of aluminum nitride was determined to be around 2.81 GPa which will be taken to be σ_0 for our modeling purposes. The transition strain rate for the specimen is computed using eqn (54) which is 1450 s^{-1}. A fracture toughness value K_{Ic} of 2.7 MPa $m^{1/2}$ is used for hot pressed aluminum nitride; see Skeele *et al.* (1993). The friction coefficients for dry contacting ceramics usually range from 0.45 to 0.75. The friction coefficient (η) for aluminum nitride is assumed to be 0.6 and the initial flaw size ($2c$) is determined using eqn (8). In the present study $2c \simeq 6$ μm which will be used throughout our calculations. The flaw size appears to be reasonable considering that the grain size is approximately 2–3 μm for the material used in the investigation. The areal density of defects f_0 is assumed to be 10^{-3} which is typical for hot pressed ceramics.

The failure criterion in eqn (52) is utilized to evaluate the failure time t_c for each strain rate with the following assumptions. The failure is assumed to be dominated by a small number of flaws and the critical length for failure is taken to be half the length of the specimen. We also assume v_m to be a third of the shear wave speed c_s which appears to be a reasonable value from the available experimental data for dynamically growing cracks in ceramics; see Deobald and Kobayashi (1992). For modeling the behavior of aluminum nitride, we take $v_m = 2100$ m s^{-1}. Since t_0 is known at various strain rates, we can now compute t_c for each strain rate and hence the compressive strength as a function of strain rate. The predictions for $\gamma = 1$ together with the available experimental data from uniaxial compressive behavior of a hot pressed aluminum nitride (Subhash and Ravichandran, 1993) are shown in Fig. 8. The model predictions compare well with the experimental data over a wide range of strain rates which suggests that our constitutive model together with the fracture criteria developed in Section 4 could be used in studying high strain rate behavior of brittle materials such as ceramics under compressive loading. An examination of the model parameters suggests that the tensile cracks are propagating at velocities in excess of 1000 m s^{-1} which seems to be consistent with data available for propagating cracks under compressive loads in ceramics; see Winkler *et al.* (1989).

5. DISCUSSION AND CONCLUSIONS

The constitutive model developed for uniaxial constant strain rate loading has been used successfully in Section 4 to explain the behavior of a hot pressed aluminum nitride

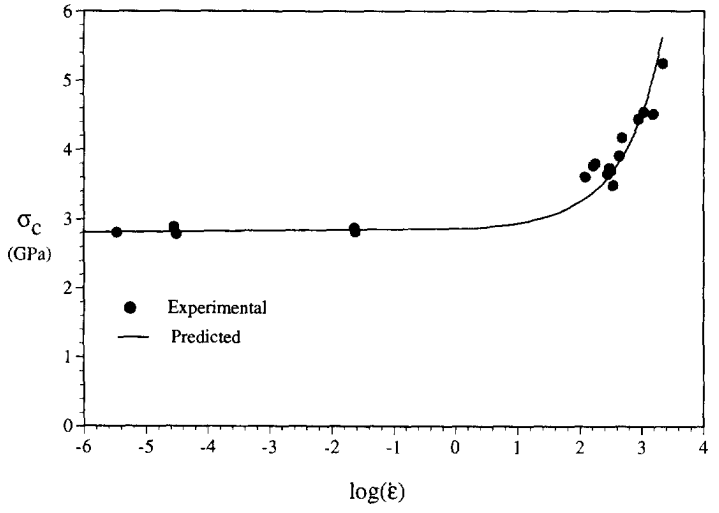

Fig. 8. Compressive strength versus strain rate for hot pressed aluminum nitride: solid line is the analytical prediction and the solid circles represent split Hopkinson (Kolsky) bar experimental data.

subjected to uniaxial compression. The model reveals that the dominant factors which influence the rate sensitivity and hence the ultimate failure strength are (a) the relation between the toughness K_{Id} and the crack velocity v and (b) the time taken to reach the critical stress intensity K_{Ic} in the vicinity of the nucleation sites, or in other words the value of the critical stress intensity factor which in turn is reflected in the quasi-static compressive strength σ_0. It appears from our model, in order for brittle materials to exhibit strong rate sensitivity, that the K_{Id}–v relationship should be a monotonically decreasing function as shown in Fig. 4. Such a relationship has been observed in brittle materials such as glass (Kobayashi *et al.*, 1983); however, in ceramics, this issue needs to be clarified further; see, for example, Yang and Kobayashi (1990).

Several assumptions have been made in constructing the constitutive model. These assumptions have been made primarily due to lack of sufficient experimental data for ceramics regarding their dynamic fracture behavior. The most serious of them appears to be the assumption that K_{Ic} is athermal and independent of loading rate. There have been suggestions (Brockenbrough *et al.*, 1988; Duffy *et al.*, 1989; Suresh *et al.*, 1990) that the initiation values for K_{Ic} under dynamic loading may be a factor of 1.27 higher than their static value for ceramics such as Al_2O_3. We have not made the distinction between static and dynamic crack initiation stress intensity factors. If definitive data were available, we could incorporate the rate dependence of the initiation value for the critical stress intensity factor in our model. In our present study we have ignored the interaction effects between cracks which appears to be reasonable for engineering ceramics where the initial flaw density f_0 is very small, of the order of 10^{-3}–10^{-2}. However, if the interaction effects become important one can accommodate them by modifying our sliding crack model to include a collinear array of cracks rather than based on non-interacting microcracks. Recently, Nemat-Nasser and Deng (1994) have considered such a scheme to understand the effect of strain rate and flaw spacing on brittle failure in compression. In our modeling we have also assumed the initial flaws to be two-dimensional slit cracks, however, one could extend the present model to three-dimensional penny-shaped cracks following the suggestions made by Ashby and Sammis (1990). A strong assumption has been made regarding the dynamic energy release rate, which is assumed to be a monotonically decreasing function of the crack velocity (see Fig. 4). This remains to be experimentally verified in ceramics by direct measurements.

The model developed for biaxial compressive loading based on the sliding crack is applicable to understanding the failure modes in brittle materials such as ceramics subjected to transient compressive loading, such as in the event of an impact of a plate by an impactor. This can be accomplished by transforming the local stress state for plane problems, i.e σ_{11}, σ_{22}, σ_{12}, into their principal stress components, i.e. σ_1 and σ_2 in the transformed coordinate system. The sliding cracks tend to grow in the direction of maximum compressive stress. The results derived here are in general applicable as long as the maximum compressive principal stress, say σ_1, is much greater in magnitude than the prevailing minimum principal stress, σ_2. By considering the magnitude of loading and prevailing local strain rates, one can adapt the results presented in Section 3 to obtain the results in the transformed coordinate system. This could provide a powerful tool for modeling and predicting failure of structures made of ceramics under impact loading conditions.

Acknowledgments—The support provided by a Presidential Young Investigator Award to G. R. from the National Science Foundation, grant No. MSS-9157846, and the matching funds provided by the Dow Chemical Company, are gratefully acknowledged. We are also pleased to acknowledge many helpful discussions with Dr Michael El-Raheb of the Dow Chemical Company, Midland, MI, and the help provided by Dr Cheng Liu in developing the constitutive model for microcracking solids under compression.

REFERENCES

Ashby, M. F. and Hallam, S. D. (1986). The failure of brittle solids containing small cracks under compressive stress states. *Acta Metal.* **34,** 497–510.

Ashby, M. F. and Sammis, C. G. (1990). The damage mechanics of brittle solids in compression. *PAGEOPH* **133,** 489–533.

Brace, W. F. and Bombolakis, E. G. (1963). A note on brittle crack growth in compression. *J. Geophys. Res.* **68,** 3709–3713.
Brockenbrough, J. R., Suresh, S. and Duffy, J. (1988). An analysis of dynamic fracture in microcracking brittle solids. *Phil. Mag.* **A58,** 619–634.
Budiansky, B. and O'Connell, R. J. (1976). Elastic moduli of cracked solids. *Int. J. Solids Structures* **12,** 81–97.
Costin, L. S. (1983). A microcrack model for deformation of brittle rock. *J. Geophys. Res.* **88,** 9485–9492.
Costin, L. S. (1987). Time dependent deformation and failure. In *Fracture Mechanics of Rock.* (Edited by B. K. Atkinson), pp. 167–216. Academic Press Geology Series, London.
Dally, J. W., Fourney, W. L. and Irwin, G. R. (1985). On the uniqueness of the stress intensity factor crack velocity relationship. *Int. J. Fracture* **27,** 159–168.
Deobald, L. R. and Kobayashi, A. S. (1992). Dynamic fracture characterization of Al_2O_3 and SiCw/Al_2O_3. *J. Am. Ceram. Soc.* **75,** 2867–2870.
Deng, H. and Nemat-Nasser, S. (1993). Dynamic damage evolution in brittle microcracking solids. *Mech. Mater.* **14,** 83–103.
Duffy, J., Suresh, S., Cho, K. and Bopp, E. R. (1988). A method for dynamic fracture initiation testing of ceramics. *J. Engng Mater.* **110,** 325–331.
Duffy, J., Suresh, S., Cho, K. and Bopp, E. R. (1989). Addendum, A method for dynamic fracture initiation testing of ceramics. *J. Engng Mater.* **111,** 86.
Evans, A. G. (1972). Slow crack growth in brittle materials under dynamic loading conditions. *Int. J. Fracture* **10,** 251–259.
Freund, L. B. (1977). A simple model of the double cantilever beam crack propagation specimen. *J. Mech. Phys. Solids* **25,** 69–79.
Freund, L. B. (1990). *Dynamic Fracture Mechanics.* Cambridge University Press, Cambridge.
Grady, D. E. (1977). Processes occurring in shock wave compression of rocks and minerals. In *High Pressure Research–Geophysical Applications* (Edited by M. H. Manghnani and S.-I. Akimoto), 389–438. Academic Press, New York.
Grady, D. E. and Lipkin, J. (1980). Criteria for impulsive rock fracture. *Geophys. Res. Lett.* **7,** 255–58.
Horii, H. and Nemat-Nasser, S. (1986). Brittle failure in compression: splitting, faulting and ductile–brittle transition. *Phil. Trans. R. Soc.* **A319,** 337–374.
Kachanov, M. (1982). Microcrack model for rock inelasticity, Part I: frictional sliding on pre-existing microcracks. *Mech. Mater.* **1,** 3–18.
Kobayashi, A. S., Emery, A. F. and Liaw, B.-M. (1983). Dynamic fracture of glass. In *Fracture Mechanics of Ceramics* (Edited by R. C. Bradt, A. G. Evans, D. P. H. Hasselman and F. F. Lange), Vol. 6. Plenum Press, New York.
Krajcinovic, D. (1989). Continuum damage mechanics. *Mech. Mater.* **8,** 117–197.
Lange, F. F. (1983). Processing related fracture origins: I, observations in sintered and isostatically hot-pressed Al_2O_3/ZrO_2 composites. *J. Am. Ceram. Soc.* **66,** 396–398.
Lankford, J. (1977). Compressive strength and microplasticity in polycrystalline alumina. *J. Mater. Sci.* **12,** 791–796.
Lankford, J. (1981). Mechanisms responsible for strain-rate dependent compressive strength in ceramic materials. *J. Am. Ceram. Soc.* **64,** C-33–C34.
Longy, F. and Cagnoux, J. (1989). Plasticity and microcracking in shock loaded alumina. *J. Am. Ceram. Soc.* **72,** 971–979.
McClintock, F. A. and Walsh, J. B. (1963). Friction on Griffith cracks under pressure. In *Proceedings of the 4th U.S. National Congress on Applied Mechanics* (1962, Vol. 2, pp. 1015–1021. ASME Press, New York.
Moss, W. C. and Gupta, Y. M. (1982). A constitutive model for describing dilatancy and failure in brittle rock. *J. Geophys. Res.* **87,** 2985–2998.
Myer, L. R., Kemeny, J. M., Zheng, Z., Suarez, R., Ewy, R. T. and Cook, N. G. W. (1992). Extensile cracking in porous rock under differential compressive stress. *Appl. Mech. Rev.* **45,** 263–280.
Nemat-Nasser, S. and Deng, H. (1994). Strain rate effect on brittle failure in compression. *Acta Metal. Mater.* **42,** 1013–1024.
Nemat-Nasser, S. and Horii, H. (1982). Compression induced nonplanar crack extension with application to splitting, exfoliation and rockburst. *J. Geophys. Res.* **87,** 6805–6821.
Nemat-Nasser, S. and Obata, N. (1988). A microcrack model of dilatancy in brittle materials. *J. Appl. Mech.* **110,** 24–35.
Ortiz, M. (1985). A constitutive theory for inelastic behavior of concrete. *Mech. Mater.* **4,** 67–93.
Palmer, A. C. and Rice, J. R. (1973). The growth of slip surfaces in the progressive failure of overconsolidated clay. *Proc. R. Soc.* **A332,** 527–548.
Raiser, G. F. and Clifton, R. J. (1993). High strain rate deformation and damage in ceramic materials. *J. Engng Mater. Tech.* **115,** 292–299.
Ramesh, K. T. and Ravichandran, G. (1990). Dynamic behavior of a boron carbide–aluminum cermet: experiments and observations. *Mech. Mater.* **11,** 19–29.
Ravichandran, G. and Chen, W. (1991) Dynamic failure of brittle materials under uniaxial compression. In *Experiments in Micromechanics of Failure Resistant Materials* (Edited by K.-S. Kim), AMD-Vol. 130, pp. 85–90. ASME Press, New York.
Ravichandran, G. and Clifton, R. J. (1989). Dynamic fracture under plane wave loading. *Int. J. Fracture* **40,** 157–201.
Rubin, A. M. and Ahrens, T. J. (1991). Dynamic tensile failure induced velocity deficits in rock. *Geophys. Res. Lett.* **18,** 219–222.
Sammis, C. G. and Ashby, M. F. (1986). The failure of brittle solids under compressive stress states. *Acta Metal.* **34,** 511–526.
Skeele, F. P., Slavin, M. J. and Katz, R. N. (1989). In *Ceramic Materials and Components for Engines* (Edited by V. J. Tennery), pp. 710–718. American Ceramic Society, Westerville, Ohio.
Subhash, G. and Nemat-Nasser, S. (1993). Dynamic stress induced transformation and texture formation in uniaxial compression of zirconia ceramics. *J. Am. Ceram. Soc.* **76,** 153–165J.

Subhash, G. and Ravichandran, G. (1993). Mechanical behavior of hot pressed aluminum nitride under uniaxial compression. SM Report No. 93-7, Graduate Aeronautical Laboratories, California Institute of Technology, Pasadena, California.

Suresh, S., Nakamura, T., Yeshuran, Y., Yang, K. H. and Duffy, J. (1990). Tensile fracture toughness of ceramic materials—effects of dynamic loading and elevated temperatures. *J. Am. Ceram. Soc.* **73,** 2457–2466.

Vekinis, G., Ashby, M. F. and Beoumont, P. W. R. (1991). *Acta Metal. Mater.* **39,** 2583–2588.

Winkler, W. D., Senf, H. and Rothenhaeusler, H. (1989). Experimental investigation of wave fracture phenomena in impacted ceramic materials. Final Report to the European Army Research Office, Contract No. DAJA45-88-C-0011.

Yang, K. H. and Kobayashi, A. S. (1990). Dynamic fracture responses of alumina and two ceramic composites. *J. Am. Ceram. Soc.* **73,** 2309–2315.

APPENDIX

The constants p_1, p_2, q_1, q_2, q_3 and q_4 in eqns (33 a–c) are functions of the friction coefficient η and are given below:

$$p_1 = \frac{1}{\pi(\pi-2\theta_s)}\{2(\pi-2\theta_s)(1+3\eta^2)+(1-\eta^2)\sin 4\theta_s - 16\eta\cos^4\theta_s - 8\eta^2\sin 2\theta_s\} \tag{A1}$$

$$p_2 = \frac{\eta}{(\sqrt{2})(\pi-2\theta_s)}\{8\cos^4\theta_s + 8\eta\sin 2\theta_s + \eta\sin 4\theta_s - 6\eta(\pi-2\theta_s)\} \tag{A2}$$

$$q_1 = -\frac{1}{\pi(\pi-2\theta_s)}\{2(\pi-2\theta_s)(1-\eta^2)+(1-\eta^2)\sin 4\theta_s + 4\eta\sin^2 2\theta_s\} \tag{A3}$$

$$q_2 = -\frac{16}{3(\pi-2\theta_s)}\{\cos^3\theta_s - 2\eta + 3\eta\sin\theta_s - \eta\sin^3\theta_s\} \tag{A4}$$

$$q_3 = -\frac{\eta}{(\sqrt{2})(\pi-2\theta_s)}\{2\eta(\pi-2\theta_s) - 2\sin^2 2\theta_s + \eta\sin 4\theta_s\} \tag{A5}$$

$$q_4 = -\frac{4(\sqrt{2}-1)\eta}{(\pi-2\theta_s)}\{1-\sin\theta_s\}, \tag{A6}$$

where

$$\theta_s = \arctan(\eta). \tag{A7}$$

A plot of the above functions as a function of the friction coefficient η is shown in Fig. A1.

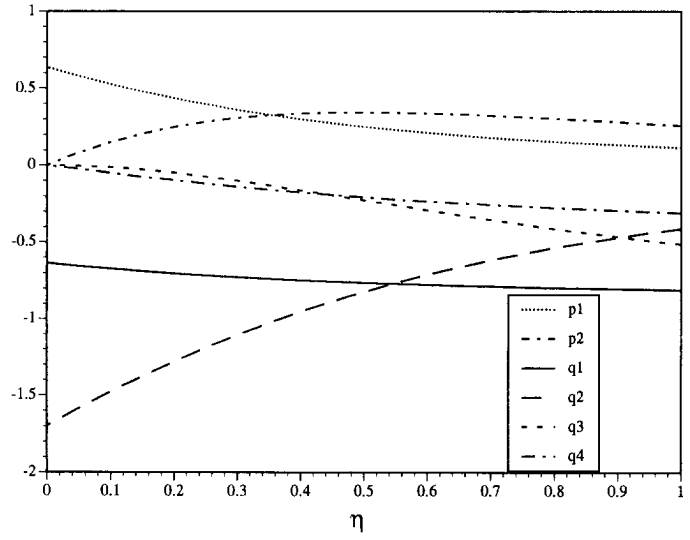

Fig. A1. The variation of coefficients p_1, p_2, q_1, q_2, q_3 and q_4 with the coefficient of friction η.